Effects of Efavirenz Binding on the Subunit Equilibria of HIV-1 Reverse Transcriptase†

Carl F. Venezia,‡ Kathryn J. Howard,§ Michael E. Ignatov,§ Leslie A. Holladay,|| and Mary D. Barkley*,‡,§

Departments of Chemistry and of Physiology and Biophysics, Case Western Reserve University, 10900 Euclid Avenue, Cleveland, Ohio 44106

Received September 20, 2005; Revised Manuscript Received December 19, 2005

ABSTRACT: Recent studies showed that nonnucleoside reverse transcriptase inhibitors (NNRTIs) have variable effects on dimerization of p66 and p51 subunits of HIV-1 reverse transcriptase (RT). Efavirenz, one of three NNRTIs currently used in highly active anti-retroviral therapy, enhances subunit dimerization. Sedimentation equilibrium experiments on each subunit and equimolar mixtures of both subunits were used to measure dissociation constants for the three coupled dimerization reactions of RT in the absence and presence of saturating concentrations of the drug. The dimerization constants of the p51/p51 homodimer, the p66/p66 homodimer, and the p66/p51 heterodimer increased 600-, 50-, and 25-fold, respectively, upon binding of efavirenz. The effects of NNRTIs on RT dimerization are consistent with a thermodynamic linkage between subunit association/dissociation and inhibitor binding. Analysis of crystal structures of the p66/p51 heterodimer reveals that efavirenz binding induces small structural changes at the dimer interface.

HIV-1[1] reverse transcriptase plays a pivotal role in HIV replication by converting single-stranded genomic RNA into double-stranded proviral DNA. The enzyme catalyzes two reactions: DNA polymerization and RNA hydrolysis. The biologically active species is a heterodimer of p66 and p51 subunits, which have the same N-terminal amino acid sequence. The p51 subunit stems from proteolytic removal of the C-terminal RNase H domain of p66 by HIV protease. Despite being an obligate feature of RT structure and function, the interactions of the two subunits have not been extensively studied. In solution, RT exists as an equilibrium mixture of monomers and dimers that include the p66/p51 heterodimer, the p66/p66 homodimer, and the p51/p51 homodimer. Monomeric species of p66 and p51 are catalytically inactive (*1*, *2*). The two enzyme active sites are in the p66 subunit of the p66/p51 heterodimer (*3*). However, both homodimers have DNA polymerase activity (*4*), and the p66/p66 homodimer also has RNase H activity (*2*). Subunit dimerization is a reversible process, with the heterodimer being the most stable. Equilibrium dissociation constants K_d of 0.4 nM to 2 μM have been reported for the p66/p51 heterodimer, compared to values of 0.4−20 μM for the p66/p66 homodimer and ∼1 mM for the p51/p51 homodimer (*1*, *5*−*10*).

The majority of AIDS drugs in clinical use target the DNA polymerase activity of RT and include nucleoside analogues and nonnucleoside RT inhibitors. The NNRTIs are a diverse group of small hydrophobic molecules that specifically inhibit HIV-1 RT (*11*, *12*). These drugs have a widening spectrum of effects on the enzyme, ranging from inhibition of DNA polymerase and RNase H activities (*13*) to perturbation of subunit interactions (*14*). Though differing in other properties, all NNRTIs are noncompetitive inhibitors that slow the chemical step in the DNA polymerization cycle by an unknown mechanism (*15*, *16*). Crystal structures of RT−NNRTI complexes show one inhibitor molecule bound to the p66/p51 heterodimer in a pocket ∼10 Å from the DNA polymerase active site (*17*−*19*). Recent studies using yeast two-hybrid assays, in vitro binding assays, urea denaturation, and size exclusion chromatography demonstrated that NNRTIs affect the dimerization of RT subunits. Efavirenz and nevirapine enhance dimerization (*14*, *20*); delaviridine has no effect (*14*), and TSAOe^{3}T, BBNH, and BBSH weaken dimerization (*8*, *9*). The significance of these effects on RT dimerization for the inhibition mechanism is not known. The NNRTI binding pocket resides almost completely in the p66 subunit of the p66/p51 heterodimer, suggesting that perturbation of the subunit interactions is indirect.

† This work was supported by NIH Grant GM52263. C.F.V. was supported by NIH Training Grant HL07653.

* To whom correspondence should be addressed. Telephone: (216) 368-0602. Fax: (216) 368-0604. E-mail: mdb4@case.edu.

‡ Department of Physiology and Biophysics.

§ Department of Chemistry.

|| Mailing address: P.O. Box 244, Townsend, TN 37881. E-mail: holladayl@aol.com.

[1] Abbreviations: ASA, accessible surface area; BBNH, *N*-(4-*tert*-butylbenzoyl)-2-hydroxy-1-naphthaldehyde hydrazone; BBSH, (4-*tert*-butylbenzoyl)-2-hydroxy-1-salicylyl hydrazone; EDTA, ethylenediaminetetraacetic acid; efavirenz, (4*S*)-6-chloro-4-cyclopropylethynyl-1,4-dihydro-4-trifluoromethyl-2*H*-3,1-benzoxazin-2-one; HIV-1, human immunodeficiency virus type 1; NNRTI, nonnucleoside reverse transcriptase inhibitor; NTA, nitrilotriacetic acid; PMSF, phenylmethanesulfonyl fluoride; PR, HIV-1 protease; RT, reverse transcriptase; SDS−PAGE, sodium dodecyl sulfate−polyacrylamide gel electrophoresis; SIS, single-ideal-species model; TCEP, tris(2-carboxyethyl)phosphine; Tris, tris(hydroxymethyl)aminomethane; TSAOe^{3}T, 1-(spiro{4-amino-2,2-dioxo-1,2-oxathiole-5,3′-[2′,5′-bis-*O*-(*tert*-butyldimethylsilyl)-β-D-ribofuranosyl]})-3-ethylthymine.

10.1021/bi051915z CCC: $33.50
Published on Web 02/10/2006

Most of the dissociation constants for RT in the literature, whether in the absence or presence of NNRTI, were determined using denaturants to dissociate dimers to folded monomers. Unfortunately, the solvent denaturation profiles of RT do not show separate transitions for dimer dissociation and monomer unfolding, creating uncertainty in the accuracy of the K_d values. Moreover, published K_d values of the p66/p51 heterodimer determined by sedimentation equilibrium (*5*, *7*) and solvent denaturation (*1*, *6*, *8*−*10*) vary over 3 orders of magnitude. Possible reasons for this range from differences in buffer composition to neglect of the multiple subunit equilibria to systematic experimental errors. Therefore, we used the thermodynamically rigorous method of sedimentation equilibrium to revisit the dissociation constants of RT. This paper reports dissociation constants of RT homo- and heterodimers determined by sedimentation equilibrium in the absence and presence of efavirenz. A thermodynamic linkage is proposed to explain the variable effects of NNRTIs on RT dimerization.

EXPERIMENTAL PROCEDURES

Materials. Efavirenz was obtained from the NIH AIDS Research and Reference Reagent Program (Germantown, MD). Oligodeoxynucleotide primers were purchased from Operon Technologies (Alameda, CA). Biochemical reagents were purchased from Roche Applied Science (Indianapolis, IN). TCEP was from Molecular Probes (Eugene, OR). Other chemicals were purchased from Sigma Chemicals (St. Louis, MO). RT buffer A/78 is 0.05 M NaH_2PO_4 (pH 7.8). RT wash buffer A/78 is RT buffer A/78 containing 1 M NaCl, 10% (v/v) glycerol, and 5−20 mM imidazole. RT buffer A/60 is 0.05 M NaH_2PO_4 (pH 6.0), 1 M NaCl, and 10% (v/v) glycerol. RT buffer D is 0.05 M Tris-HCl (RNase, DNase-free, pH 7.0), 25 mM NaCl, 1 mM EDTA, and 10% (v/v) glycerol (molecular biology grade redistilled). Storage buffer D is RT buffer D containing 50% (v/v) glycerol. TBE buffer is 0.089 M Tris, 0.089 M boric acid (pH 8.0), and 2 mM EDTA.

Cloning. The C38V/C280S double mutation was introduced into the p6H RT-PR plasmid by two rounds of mutagenesis using the QuikChange site-directed mutagenesis kit (Stratagene, La Jolla, CA). Mutagenic oligonucleotide primer sequences for the C38V mutation were as follows: forward, 5′-GGCCATTGACAGAAGAAAAAATAAAAG-CATTAGTAGAAATT**GTG**ACAGAAATGGAAAAGG-AAGGG-3′; reverse, 5′-CCCTTCCTTTTCCATTTCTGT-**CAC**AATTTCTACTAATGCTTTTATTTTTTCTTCTGT-CAATGGCC-3′. Primer sequences for the C280S mutation were as follows: forward, 5′-CCCAGGGATTAAAGTAA-GGCAATTA**AGT**AAACTCCTTAGAGGAACCAAAGC-3′; reverse, 5′-GCTTTGGTTCCTCTAAGGAGTTT**ACT**-TAATTGCCTTACTTTAATCCCTGGG-3′. The C38V/C280S mutation was transferred into p6H RT and p6H RT51 plasmids using restriction enzyme digestion and DNA ligation. For the p6H $RT^{C38V/C280S}$ plasmid, p6H RT and p6H $RT^{C38V/C280S}$-PR were digested separately with BamHI and HindIII. For the p6H $RT51^{C38V/C280S}$ plasmid, p6H $RT51^{C280S}$ and p6H $RT^{C38V/C280S}$-PR were digested separately with BamHI and EcoRV. Restriction fragments were separated on a 1% agarose gel in TBE buffer, followed by purification, DNA ligation, and transformation. All mutations were confirmed by DNA sequencing at Cleveland Genomics (Cleveland, OH).

Table 1: HIV-1 RT Proteins

	p66	p51	p66/p51
molecular mass (kDa)	66481	53229	119710
extinction coefficient at 280 nm (M^{-1} cm^{-1})	136270	124180	130225[a]
fringe factor	2.713	2.733	2.722
buoyancy factor ($1 - \bar{v}\rho$)	0.251	0.251	0.251

[a] Concentration expressed as monomer. For concentrations expressed as dimer, the value is 260450.

Protein Purification. HIV-1 RT proteins with N-terminal hexahistidine extensions were produced using three plasmids: p6H RT-PR for the p66/p51 heterodimer, p6H RT for p66, and p6H RT51 for p51. Authentic p66/p51 heterodimer without the His tags was produced using pRT AUTH-PR. RT proteins were purified as described previously (*21*) with the following modifications. Complete, EDTA-free protease inhibitor cocktail tablets (1 tablet per 50 mL of lysate) were used instead of PMSF; 1 M NaCl was added to the lysate before sonication for six 30 s pulses in a VCX 600 ultrasonic processor (Sonics & Materials, Newton, CT), and 20 mM imidazole was added to the lysate after centrifugation. Ni−NTA Superflow resin (Qiagen, Valencia, CA) was equilibrated with RT wash buffer A/78 to minimize nonspecific binding. After loading, the Ni−NTA column was washed with 1 column volume of RT wash buffer A/78 and then with RT buffer A/60 containing 20 mM imidazole. The Ni−NTA column was eluted with a 15 column volume gradient of 20 to 500 mM imidazole; fractions were analyzed by SDS−PAGE, and the pooled fractions were dialyzed into RT buffer D. The S-Sepharose column was run after the Ni−NTA column. Pooled fractions from the S-Sepharose column were dialyzed into RT buffer D at pH 8.2 before DEAE chromatography. Sucrose was used as a concentration step prior to dialysis into storage buffer D. Proteins were >95% pure as judged by SDS−PAGE. The protein concentration is determined from absorbance at 280 nm A_{280} using extinction coefficients in Table 1. All RT protein concentrations are expressed as monomer.

Sedimentation Equilibrium. Sedimentation equilibrium experiments were performed on a Beckman XL-I analytical ultracentrifuge. Protein samples (1 mL) were dialyzed overnight against 2 × 0.5 L of RT buffer D containing 1 mM TCEP at 4 °C. The presence of 10% glycerol in the buffer increases solvent viscosity, resulting in a 1.4-fold increase in time to equilibrium compared to that in water. For experiments in the presence of inhibitor, 25 μM efavirenz was added to the dialysis buffer. The protein sample (0.27 mL) and dialysate buffer (0.3 mL) were loaded into a cell with a 12 mm double-sector EPON centerpiece and sapphire windows. The long solution column was used to increase the information content of the data. Assuming a rectangular cell and constant field in the approximation of van Holde and Baldwin (*22*), the increase in solution volume from the usual 0.1 mL to 0.27 mL would increase the time to equilibrium by ∼6-fold. Three cells and a counterbalance were run in a four-hole rotor at 8−16 × 10^3 rpm and 5 °C. Runs were made at several protein concentrations and speeds. Equilibrium was established by comparing 12 scans at 2 h intervals at each speed. Typical equilibration times were 1

week for the initial lowest rotor speed and 3−4 days for subsequent higher rotor speeds. Absorption data and interference data were collected for all runs. Absorbance was monitored at 280 nm. For protein concentrations of $\leq 3\ \mu$M, only absorption data were analyzed; for concentrations of $\geq 6\ \mu$M, only interference data were analyzed. At the end of a run, protein samples were removed from the cell and analyzed by SDS−PAGE; no evidence of protein degradation was observed.

Data files were examined in XLGraph (*23*) to determine the region of interest and were trimmed using a conversion program, which also removes an occasional errant data point (three standard deviations from the average of 10 adjacent points). A baseline was subtracted from interference scans to zero the first data point at the top of the solution column. Protein parameters used in the data analysis are given in Table 1. The molecular weight and extinction coefficient at 280 nm ϵ_{280} were calculated from the amino acid sequence (*24*). The ϵ_{280} value of the p66/p51 heterodimer was confirmed by amino acid analysis (*25*). Partial specific volume $\bar{v}$ and fringe factor *ff*, where *ff* is the number of fringes per milligram per milliliter per 1.0 cm path length at 675 nm (see the Supporting Information), were calculated in PROTCALC (*26*), using the Privalov database (*27*). The effect of 10% glycerol on the effective partial specific volume of proteins is 0.4−0.8% (*28*), which is smaller than the error in computing the partial specific volume from the various published databases. Solvent density ρ was measured on an Anton Paar DMA 5000 density meter (Graz, Austria).

Data Analysis. Data sets were first fit to a single-ideal-species model. Samples with cell average weight-average molecular weight $M_w$cell or SIS molecular weight intermediate between monomer and dimer were analyzed further as associating systems. Data sets for p66 and p51 were fit to a self-association model using MIXEDFIT (*26*) with the monomer molecular weight fixed. In addition to determining the self-association model (fixed self-associating or isodesmic), this program was used to obtain multimer stoichiometry and equilibrium constants. After the self-associations of p66 and p51 were characterized separately, data sets for the p66/p51 heterodimer were analyzed with HETERFIT (*26*) to determine the heterodimer association constant. Such samples may contain both p66/p66 and p51/p51 homodimers as well as the p66/p51 heterodimer. The self-association constants for both homodimers as well as the monomer molecular weights were fixed at known values in the model equations.

$M_w$cell was determined for individual absorbance scans with MWCALC using a spline fit of ln(absorbance) versus radius squared (*26*, *29*). Absorbance or interference data at multiple rotor speeds were analyzed by nonlinear least squares using the following procedures in MIXEDFIT. The fitting metric for absorbance data analyses was the weighted L1 norm suggested by Lewis and Dimitriadis (*30*). Four data files at each of three speeds were fit in a global analysis to

$$A(r) = \epsilon_{280} M_1 l \sum_{1}^{n+1} \exp(Wa_i) + A_{base} \qquad (1a)$$

where $A(r)$ is the absorbance at radial distance r, A_{base} is the nonsedimenting absorbance, M_1 is the monomer molecular weight, l is the path length of the centrifuge cell, and Wa_i is given by

$$Wa_i = \ln(L_i K_i) + L_i\{\ln C_1(F) + A' M_1(1 - \bar{v}\rho)(r^2 - F^2) - BM_1[A(r) - A(F)]/(\epsilon_{280} l)\} \qquad (1b)$$

where L_i and K_i are the number of monomers and the equilibrium association constant for the *i*mer, respectively. L_1 and K_1 are unity. F is the reference distance at 70% of the radial distance between the top a and bottom b of the solution column. $C_1(F)$ is the molar concentration of monomer when $r = F$. $A' = \omega^2/(2RT)$, where ω is angular velocity in inverse seconds, R is the gas constant, and T is the absolute temperature. B is the second virial coefficient in moles liter per square gram.

Interference data were fit with the L_2 least squares metric to

$$\Delta\text{fringe}(r) = -J_a + ffM_1 l \sum_{1}^{n+1} \exp(Wf_i) \qquad (2a)$$

where $\Delta\text{fringe}(r) = J(r) - J(a)$ is the relative fringe shift at r, $J(a)$ is the concentration when $r = a$ in units of fringe, and Wf_i is given by

$$Wf_i = \ln(L_i K_i) + L_i[\ln C_1(F) + A' M_1(1 - \bar{v}\rho)(r^2 - F^2) - BM_1 \Delta\text{fringe}/(ffl)] \qquad (2b)$$

Because interference optics measure only $\Delta\text{fringe}(r)$, it is necessary to introduce the nuisance parameter $J(a)$ into the fitting procedure for a given data set and cell. An initial guess for $J(a)$ may be obtained from the interference data by equating eqs 3 and 4, the expressions for conservation of mass

$$J(a) = J_0 - [2/(b^2 - a^2)]\int_a^b [J(r) - J(a)] r\, dr \qquad (3)$$

where J_0 is the initial concentration in units of fringe, and for a single ideal species

$$J(a) = \Delta J/[\exp(\Delta J/J_0) - 1] \qquad (4)$$

where $\Delta J = J(b) - J(a)$ is the increase in fringes from the top to the bottom of the solution column. The resulting nonlinear equation is solved by Newton's method for J_0, the only unknown (*31*). The program estimates an initial guess for $J(a)$ using eq 3 or 4. For some data sets, this algorithm will fail and return a negative value for J_0; if so, the default initial guess for $J(a)$ is 0.2 fringe. For a single-ideal-species model, the initial guess for $J(a)$ is excellent. For self-association models, the estimate for $J(a)$ is generally too small by a factor of 2 or 3. Therefore, the data analysis begins by fitting only the data at the highest speed to the self-association model; the value of $J(a)$ tends to be quite small, and the initial guess is not too important. Once the highest-speed data have been well fit, the data at the next lower speed are added and the fit is redone, retaining the best values of the parameters for the highest-speed data as the initial guesses of those parameters in the next round. This process is then repeated until all the data are combined in a single global fit. In practice, this protocol shortens the total computational

time and reduces the extent of trapping of the Simplex minimization algorithm in local minima.

Standard errors of parameters were obtained with 100 trials of the balanced bootstrap algorithm; 95% confidence intervals were computed using two standard deviations from the estimated parameter value.

Mathematica Calculations. The concentration of the five forms of RT in a solution of the p66/p51 heterodimer was calculated using Mathematica 5 (Wolfram Research). The following set of five equations represents the three dimer dissociation constants and two mass balance equations

$$K_d(\text{p51/p51}) = [\text{p51}]^2/[\text{p51/p51}] = A^2/AA \quad (5)$$

$$K_d(\text{p66/p66}) = [\text{p66}]^2/[\text{p66/p66}] = B^2/BB \quad (6)$$

$$K_d(\text{p66/p51}) = [\text{p66}][\text{p51}]/[\text{p66/p51}] = A^*B/AB \quad (7)$$

$$[\text{p51}]_{tot} = [\text{p51}] + 2[\text{p51/p51}] + [\text{p66/p51}] = A_0 = A + 2AA + AB \quad (8)$$

$$[\text{p66}]_{tot} = [\text{p66}] + 2[\text{p66/p66}] + [\text{p66/p51}] = B_0 = B + 2BB + AB \quad (9)$$

where K_d(p51/p51), K_d(p66/p66), and K_d(p66/p51) are equilibrium dissociation constants of p51/p51, p66/p66, and p66/p51 dimers, respectively, and $[\text{p51}]_{tot}$ and $[\text{p66}]_{tot}$ are total concentrations of p51 and p66, respectively. This set of equations is then solved using a built-in function to produce four possible sets of closed-form solutions:

solve[{eq 5,eq 6,eq 7,eq 8,eq 9},{*A*,*B*,*AA*,*BB*,*AB*}]

Each solution set is tested for physical plausibility. A set of equations for the concentrations of the five RT forms is obtained as a function of the total concentration of each subunit and the three dissociation constants. The p66/p51 heterodimer has a 1:1 ratio of p66 and p51, so $A_0 = B_0$. Numerical values for the dissociation constants are introduced; B_0 is set equal to A_0, and the solution set is reevaluated to simplify the equations. Numerical solutions are easily obtained for a range of protein concentrations with an arbitrary step size using a built-in function of Mathematica:

N[table[{*A*,*B*,*AA*,*BB*,*AB*},{A_0,A_0first,A_0last,A_0step}]]

Molecular Modeling. Coordinates for the following structures were obtained from the RCSB Protein Data Bank. For unliganded HIV-1 RT: 1HMV, pH 6.8, space group *C*2(*C*121) (*32*); and 1DLO, pH 6.8, space group *C*2(*C*121) (*33*). For the HIV-1 RT−efavirenz complex: 1FK9, pH 5.0, space group $P2_12_12_1$ (*18*); and 1IKW, pH 7.2, space group $C222_1$ (*19*). Several amino acids were deleted from the unliganded RT structures to permit comparison of the same amino acids in structures with and without efavirenz. Molecular graphics were performed with Deep View/Swiss-Pdb Viewer (*34*). RT structures with and without efavirenz were superimposed using the Magic Fit option for all atoms. Dimer interfaces were analyzed with the Protein−Protein Interaction Server (*35*). Interface parameter definitions are available on the Web site.

RESULTS

Sedimentation Equilibrium Analysis of Subunit Equilibria. RT subunits undergo three coupled dimerization reactions, namely, formation of p66/p51, p66/p66, and p51/p51 dimers.

$$\text{p66} + \text{p51} = \text{p66/p51} \quad (10)$$

$$\text{p66} + \text{p66} = \text{p66/p66} \quad (11)$$

$$\text{p51} + \text{p51} = \text{p51/p51} \quad (12)$$

Accurate determination of dissociation constants for associating systems requires detectable amounts of both monomeric and associated species. Obviously, if the protein concentration is too high, only associated species will be present and the apparent K_d values will represent upper limits. For our sedimentation equilibrium experiments, appropriate protein concentrations were established through a combination of literature K_d values, Mathematica calculations, and trial and error. At 0.2 μM monomer, the data were too noisy to analyze, setting a lower limit for detection of RT with absorption optics at 280 nm. All experiments were performed in RT buffer D at 5 °C, conditions under which RT is stable and soluble (>1 mM).

Sedimentation equilibrium experiments with p66 were run at three protein concentrations and three rotor speeds. One scan at each speed was analyzed to estimate $M_w$cell values for each sample (Table 2). All values fell in the molecular mass range between the 66 kDa monomer and the 132 kDa homodimer, indicating the presence of both monomeric and dimeric species and confirming proper protein concentrations for equilibrium constant determination. A fixed self-associating monomer−dimer model gave reasonable weighted-average absolute residuals and random residual plots for all p66 data. Figure 1 shows the absorbance scans and residuals for a 3.8 μM sample of p66. For a sample of a given protein concentration, four scans at each of three speeds were analyzed globally to estimate ln K_a, where K_a is the dimer association constant. The average value of ln K_a for different samples was used to calculate the dimer dissociation constant $K_d = 1/K_a$.

Because the ionic strength of the buffer (~0.05) and the computed net charge on p66 (+9) and p51 (+5) at pH 7 are low, the possibility of solution nonideality had to be evaluated (*36*). Thus, global analyses were done for both ideal and nonideal monomer−dimer models using data sets trimmed to different A_{280} limits. Table 3 shows the results for two p66 samples trimmed to include the highest absorbance data. The effect on ln K_a values of trimming the cell data at various points below the highest absorbance level (not shown) or of including a term for solution nonideality (Table 3) was negligible. Thus, the ln K_a values for p66 were obtained using data sets in which $A_{280} \leq 2.3$ and the

Table 2: Apparent Molecular Mass Averages in Wild-Type p66 Experiments

[monomer] (μM)	rotor speed (rpm)	$M_w$cell (kDa)	average absolute residual
3.8, sample 1	8×10^3	77.3	0.0099
	10×10^3	96.9	0.0050
	12×10^3	97.1	0.0063
3.8, sample 2	8×10^3	76.2	0.0119
	10×10^3	85.3	0.0056
	12×10^3	87.8	0.0074
5.2	8×10^3	85.1	0.0369
	10×10^3	90.8	0.0135
	12×10^3	95.9	0.0207

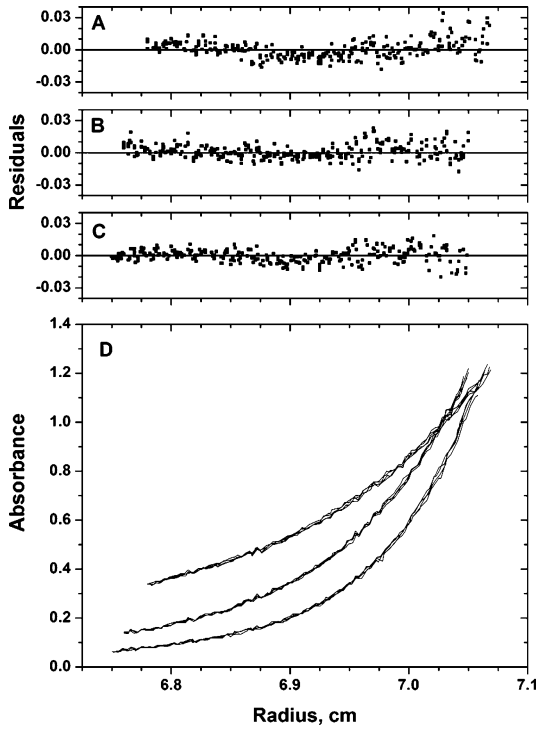

FIGURE 1: Sedimentation equilibria of 5.2 μM wild-type p66 at three rotor speeds. (A−C) Residuals for a fit to a fixed self-associating monomer−dimer ideal model at 8, 10, and 12 $\times$ 10^3 rpm, respectively. (D) Four absorbance scans of the concentration distribution at (top curve) 8 $\times$ 10^3 rpm, (middle curve) 10 $\times$ 10^3 rpm, and (bottom curve) 12 $\times$ 10^3 rpm in 0.05 M Tris (pH 7.0), 25 mM NaCl, 1 mM EDTA, and 10% (v/v) glycerol at 5 °C.

thermodynamically ideal model. Estimates for ln K_a have a close to normal distribution (*30*). The mean and standard deviation of ln K_a values obtained for the three p66 samples were computed and used to calculate a dissociation constant K_d(p66/p66) of 4.2 $\pm$ 0.8 μM for the p66/p66 homodimer (Table 4).

Previous analytical ultracentrifugation studies of HIV-1 RT proteins were limited to absorption optics and lower protein concentrations (*5*, *7*). We monitored the weak dimerization of p51 via the refractive index. Sedimentation equilibrium experiments were run at three rotor speeds on our most concentrated solution of p51. Figure 2 shows the interference data and residuals for an 80 μM sample of p51. As for p66, all p51 data were best fit by a fixed self-associating monomer−dimer model. The interference scans were initially trimmed to keep all the data at the bottom of the cell, including a linear portion of the curve at high fringe values. The fits did not converge if all the cell data were included, and the results were not reproducible if too much data were excluded. Therefore, the data were trimmed by trial and error to remove the linear portion of the curve and achieve convergence with the maximum number of data points. Table 3 shows the final results of global analyses for two p51 samples using an ideal and nonideal monomer−dimer model. The dissociation constant K_d(p51/p51) of 230 $\pm$ 30 μM for the p51/p51 homodimer is 55-fold higher than the K_d(p66/p66) for the p66/p66 homodimer (Table 4).

Sedimentation equilibrium experiments were run on an equimolar mixture of p66 and p51 at two protein concentrations and three rotor speeds. Figure 3 shows the absorbance scans and residuals at a total monomer concentration $[\text{monomer}]_{tot}$ of 0.5 μM (0.25 μM p66 and 0.25 μM p51). The data were best fit by a fixed hetero-associating monomer−dimer model with the previously determined values of the

Table 3: Solution Ideality in Wild-Type p66 and p51 Experiments[a]

RT protein	A_{280} or fringe limit	model	ln K_a	BM_1 (L g^{-1})	average absolute residual
3.5 μM p66	1.8	ideal	12.26 $\pm$ 0.05		0.0129
		nonideal	12.58 $\pm$ 0.04	0.089 (0.079−0.099)	0.0118
5.2 μM p66	2.3	ideal	12.22 $\pm$ 0.04		0.0112
		nonideal	12.46 $\pm$ 0.03	0.051 (0.042−0.062)	0.0107
80 μM p51, sample 1	12	ideal	8.27 $\pm$ 0.03		0.0877
		nonideal	8.25 $\pm$ 0.03	0.004 (0.003−0.005)	0.0907
80 μM p51, sample 2	14	ideal	8.25 $\pm$ 0.03		0.115
		nonideal	8.54 $\pm$ 0.03	0.047 (0.046−0.048)	0.0603

[a] Results from global analyses of data from experiments at 8, 10, and 12 $\times$ 10^3 rpm. Errors are 95% confidence limits or intervals.

Table 4: Dissociation Constants[a]

dimer	[monomer] (μM)	ln K_a	K_d (μM)
p66/p66 homodimer			
wild type	3.5, 3.8, 5.2	12.4 $\pm$ 0.2	4.2 $\pm$ 0.8
C38V/C280S	1.0	12.3 $\pm$ 0.03	4.4 $\pm$ 0.1
wild type with efavirenz	1.0, 2.0	16.4 $\pm$ 0.1	0.079 $\pm$ 0.008
p51/p51 homodimer			
wild type	80	8.3 $\pm$ 0.1	230 $\pm$ 30
C38V/C280S	48	6.0 $\pm$ 0.1	2400 $\pm$ 200
wild type with efavirenz	0.6	14.8 $\pm$ 0.3[b]	0.37 (0.28−0.50)[b]
p66/p51 heterodimer			
wild type	0.4, 0.5	15.0 $\pm$ 0.2	0.31 $\pm$ 0.06
authentic[c]	0.6	15.0 $\pm$ 0.2	0.31 $\pm$ 0.06
C38V/C280S	0.8	15.3 $\pm$ 0.3	0.23 $\pm$ 0.07
wild type with efavirenz	0.5	18.3 $\pm$ 0.2	0.012 $\pm$ 0.002

[a] In 0.05 M Tris-HCl (pH 7.0), 25 mM NaCl, 1 mM EDTA, 1 mM TCEP, and 10% glycerol at 5 °C. Errors are standard deviations from results of global analysis of 3−12 data sets consisting of four scans at each of three rotor speeds. [b] The error is the 95% confidence limit or interval.[c] RT with no His tags.

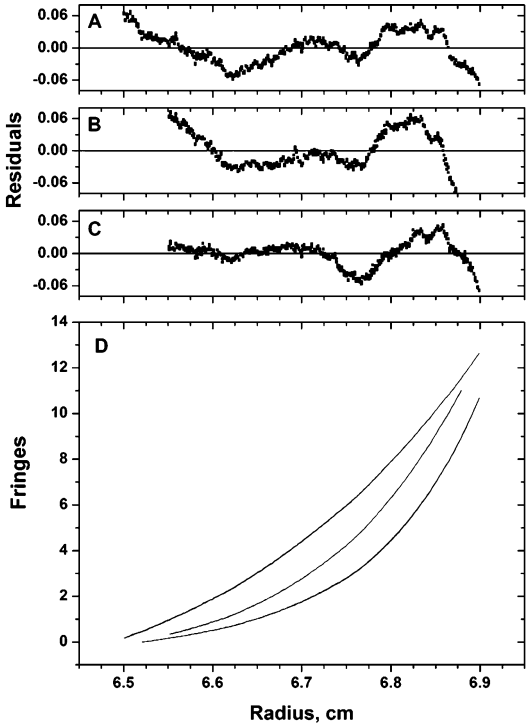

FIGURE 2: Sedimentation equilibria of 80 μM wild-type p51 at three rotor speeds. (A−C) Residuals for a fit to a fixed self-associating monomer−dimer ideal model at 8, 10, and 12 $\times$ 10^3 rpm, respectively. (D) Four interference scans of the concentration distribution at (top curve) 8 $\times$ 10^3 rpm, (middle curve) 10 $\times$ 10^3 rpm, and (bottom curve) 12 $\times$ 10^3 rpm in 0.05 M Tris (pH 7.0), 25 mM NaCl, 1 mM EDTA, and 10% (v/v) glycerol at 5 °C.

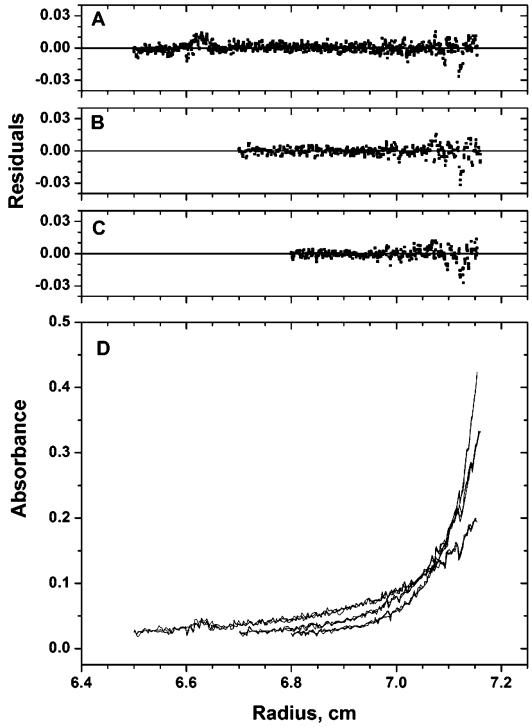

FIGURE 3: Sedimentation equilibria of an equimolar mixture of wild-type p66 and p51 (total concentration of 0.5 μM) at three rotor speeds. (A−C) Residuals for a fit to a fixed hetero-associating monomer−dimer model at 10, 13, and 16 $\times$ 10^3 rpm, respectively. (D) Four absorbance scans of the concentration distribution at (top curve) 10 $\times$ 10^3 rpm, (middle curve) 13 $\times$ 10^3 rpm, and (bottom curve) 16 $\times$ 10^3 rpm in 0.05 M Tris (pH 7.0), 25 mM NaCl, 1 mM EDTA, and 10% (v/v) glycerol at 5 °C.

self-association constants of p66 and p51 as fixed constants in HETERFIT. The dissociation constant K_d(p66/p51) of 0.31 $\pm$ 0.06 μM for the p66/p51 heterodimer is a factor of 14 lower than the K_d(p66/p66) for the p66/p66 homodimer (Table 4). In addition, experiments were run at three rotor speeds on an equimolar mixture of authentic subunits without the N-terminal His tags. The self-association constants of His-tagged p66 and p51 were used in HETERFIT to analyze the data for the equimolar mixture of authentic p66 and p51 at $[\text{monomer}]_{tot} = 0.6$ μM. The K_d(p66/p51) value calculated for the authentic p66/p51 heterodimer is identical to the value obtained for the His-tagged heterodimer. Thus, the His tags have no apparent effect on RT dimerization (Table 4).

Some of the crystal structures of the p66/p51 heterodimer were determined on RTs lacking one or both of the two wild-type cysteines, C38 and C280. The RTs used in crystal structures of the unliganded p66/p51 heterodimer have essentially the same amino acid sequence as our wild-type RT: five amino acid changes in 1HMV (*32*) and three amino acid changes in 1DLO (*33*). These conservative amino acid substitutions include C280S in 1DLO that removes one of the two cysteines. The residue at position 280 of the p51 subunit is in the dimer interface of the p66/p51 heterodimer. The site-specifically labeled heterodimers used for EPR, photo-cross-linking, and fluorescence studies had one or both wild-type cysteines replaced with serine or valine in both subunits (*37*−*41*). To test the effect of the two cysteines on dimerization, we performed sedimentation equilibrium experiments on the C38V/C280S double mutant. The dissociation constants of the $p66^{C38V/C280S}$/$p66^{C38V/C280S}$ homodimer [K_d(p66/p66) = 4.4 $\pm$ 0.1 μM] and of the $p66^{C38V/C280S}$/$p51^{C38V/C280S}$ heterodimer [K_d(p66/p51) = 0.23 $\pm$ 0.07 μM] are about the same as the values obtained for wild-type dimers (Table 4). However, the dissociation constant [K_d(p51/p51) = 2400 $\pm$ 200 μM] for the $p51^{C38V/C280S}$/$p51^{C38V/C280S}$ homodimer is ~10-fold higher than the value for the wild-type homodimer. These results suggest that the dimer interfaces in the mutant p66/p66 homodimer and p66/p51 heterodimer, but not in the mutant p51/p51 homodimer, are essentially wild-type interfaces.

Effects of Efavirenz Binding. Dissociation constants of p66/p66, p51/p51, and p66/p51 dimers were also determined in the presence of efavirenz. Sedimentation equilibrium experiments were run on solutions of p66, p51, and equimolar mixtures of p66 and p51 containing saturating levels of efavirenz, and the absorbance data were analyzed as described above. The concentrations of p66 and p51 were reduced for experiments in the presence of inhibitor to attain detectable amounts of monomeric species. The concentration used for the equimolar mixture of p66 and p51 remained the same, near the 0.2 μM detection limit of RT with absorption optics. Figure 4 shows absorbance scans of the equimolar mixture of p66 and p51 in the absence and presence of efavirenz. The shape of the concentration gradient depends on the molecular masses and dissociation constants of the associating species, with the lower concentrations at the top of the cell favoring monomers and the higher concentration at the bottom of the cell favoring dimers. The noticeable shift in the concentration gradient to the bottom of the cell in the presence of efavirenz indicates enhanced dimerization. The data sets for p66, p51, and the

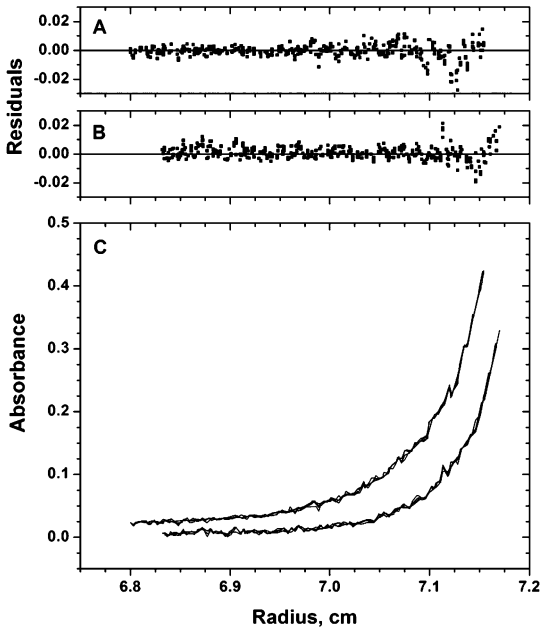

FIGURE 4: Sedimentation equilibria of an equimolar mixture of wild-type p66 and p51 (total concentration of 0.5 μM) in the absence and presence of 25 μM efavirenz at 16 $\times$ 10^3 rpm and 5 °C. (A and B) Residuals for a fit to a fixed hetero-associating monomer−dimer model in the absence and presence of efavirenz, respectively. (C) Four absorbance scans of the concentration distribution in the (top curve) absence and (bottom curve) presence of efavirenz in 0.05 M Tris (pH 7.0), 25 mM NaCl, 1 mM EDTA, and 10% (v/v) glycerol at 5 °C.

equimolar mixture of p66 and p51 in the presence of inhibitor were best fit by a fixed monomer−dimer model, but with much lower dissociation constants than in the absence of inhibitor (Table 4). A K_d(p51/p51−I) of 0.37 (0.28−0.50) μM, a K_d(p66/p66−I) of 0.079 ± 0.008 μM, and a K_d(p66/p51−I) of 0.012 ± 0.002 μM correspond to ~600-, ~50-, and ~25-fold enhancement of dimerization for p51/p51, p66/p66, and p66/p51 dimers, respectively, bound by inhibitor I. The experiment with p51 in the presence of efavirenz used a monomer concentration similar to K_d(p51/p51−I), whereas the experiments with p66 and the equimolar mixture of p66 and p51 used monomer concentrations ~10−40-fold greater than K_d(p66/p66−I) and K_d(p66/p51−I). This raised questions about the accuracy of the latter K_d values. If, for example, one species is essentially absent, no reliable estimate of K_d is possible. Using the $[monomer]_{tot}$ and K_d values in Table 4 in the dimerization reactions in eqs 10−12, we calculated 13−18 and 18% total monomer by mass in the solutions of p66 and the equimolar mixture of p66 and p51, respectively. We also computed the monomer and dimer concentrations at the reference radial distance F in the cells at equilibrium. These calculations showed that the amount of monomer by mass ranged from 5 to 15% depending on rotor speed, consistent with the values obtained from equilibrium calculations. These results, along with the error estimates, suggest that the K_d values for the three dimers in the presence of efavirenz are sufficiently robust.

DISCUSSION

Equilibrium Dissociation Constants of RT. Our K_d values in the absence of efavirenz fall within range of literature values for RT dimers (Table 4). The K_d(p66/p51) of 310 ± 60 nM at pH 7.0 and 5 °C is 20−800-fold higher than the values of 8−13 and 0.4 nM determined by acetonitrile denaturation at pH 6.5 and pH 8.0, respectively, and 25 °C, assuming two-state reversible dissociation of the p66/p51 heterodimer to folded p66 and p51 monomers (*6*). However, it is only 2−4-fold higher than the values of 150 and 76 nM at pH 7.5 determined by urea denaturation (*8*, *9*). On the other hand, our K_d(p66/p51) value is lower by a factor of 6 than the value of 1.9 μM determined by sedimentation equilibrium at pH 7.0 and 5 °C (*7*). All of these studies neglected the multiple subunit equilibria and fit the data to a self-associating monomer−dimer model. Fitting our sedimentation equilibrium data for equimolar mixtures of p66 and p51 as a self-association of pseudomonomers with a mass equal to the average of p66 and p51 overestimates K_d(p66/p51) by ~4-fold (*7*). A K_d(p66/p51) value of 2.0 μM at pH 6.5 and 5 °C was reported for sedimentation equilibrium data fit to the multiple subunit equilibria in eqs 10−12 (*5*). Dimerization of HIV-1 RT is independent of pH 7−8.5, but the extent decreases at pH <7.0 (*6*). The lower pH used in the previous sedimentation equilibrium study may account for most of the difference from our K_d(p66/p51) value.

Our K_d(p66/p66) of 4.2 ± 0.8 μM at pH 7.0 and 5 °C is 2−10-fold higher than the values of 2.0 and 0.45 μM determined by acetonitrile denaturation at pH 8.0 and 25 °C (*6*, *10*), only 1.5-fold higher than the value of 2.7 μM determined by urea denaturation at pH 7.5 and 25 °C (*9*, *10*), and equal to the value of 4.3 μM determined by gel filtration at pH 7.8 and 0 °C (*1*). Thus, it appears that solvent denaturation underestimates K_d values for the p66/p66 homodimer and probably also the p66/p51 heterodimer, acetonitrile more so than urea. A K_d(p66/p66) value of 20 μM at pH 6.5 and 5 °C was determined by sedimentation equilibrium (*5*). Here too, the difference from our K_d(p66/p66) value may be attributed to the lower pH. Finally, our K_d(p51/p51) of 230 ± 30 μM at pH 7.0 and 5 °C is smaller than the only literature value of 670 μM determined by gel filtration at pH 7.8 and 0 °C by a factor of 3 (*1*). No p51/p51 homodimer was detectable in previous sedimentation equilibrium studies (*5*).

For a solution of RT, the concentrations of the three dimeric and two monomeric species can be calculated from the three coupled dimerization reactions in eqs 10−12 using eqs 5−9 and the values for the three dissociation constants in Table 4. Figure 5 shows the percentages of the five species present in a RT solution equimolar in p66 and p51 as a function of $[monomer]_{tot}$. When $[monomer]_{tot}$ = 1 μM, [p66/p51] = 220 nM, [p66/p66] = 15 nM, [p51/p51] = 0.51 nM, [p66] = 250 nM, and [p51] = 280 nM; 44% of the total monomer is a heterodimer. When $[monomer]_{tot}$ = 10 μM, [p66/p51] = 3.7 μM, [p66/p66] = 0.19 μM, [p51/p51] = 0.011 μM, [p66] = 0.90 μM, and [p51] = 1.3 μM; 74% of the total monomer is a heterodimer. Because [p51/p51] is negligible in this concentration range (0.1% at 1 μM monomer and 0.2% at 10 μM monomer), omitting the p51 homodimerization reaction in eqs 5 and 12 has negligible effects on the calculated concentrations of monomers and the other two dimers. On the other hand, ignoring the multiple subunit equilibria completely and calculating the concentrations of heterodimer and monomers for the single dimerization reaction in eq 10 using eq 7 and the K_d(p66/p51) value of 0.31 μM overestimate the extent of dimeriza-

tion by 1.5-fold when $[RT]_{tot} = 1\ \mu M$ and 1.2-fold at 10 μM. A 1 μM RT solution would have [dimer] = 340 nM and [monomer] = 320 nM or 68% of total monomer as a heterodimer, and a 10 μM RT solution would have [dimer] = 4.4 μM and [monomer] = 1.2 μM or 88% of the total monomer as a heterodimer. Thus, for accurate values of species concentrations, the p66 homodimerization reaction as well as the heterodimerization reaction should be included in the calculations.

Effects of Efavirenz Binding on Dissociation Constants. Efavirenz is a second-generation NNRTI, which inhibits HIV-1 RT with an inhibition constant K_i of 3 nM and inhibits virus spread in cell culture with a 95% inhibition concentration IC_{95} of 1.5 nM (*42*). K_d values for binding of efavirenz to different catalytic forms of RT have been derived from steady-state kinetics: 170 nM for RT, 30 nM for RT−primer/template, and 4 nM for RT−primer/template−dNTP (*43*). Thus, RT is likely saturated with inhibitor after dialysis into 25 μM efavirenz. Binding of efavirenz stabilizes RT dimers by as much as 600-fold at pH 7.0 and 5 °C (Table 4). The order of stability of the three dimeric species in the presence of efavirenz parallels the order in the absence of inhibitor, but the relative differences in dimer stability are smaller in the inhibitor complexes. Efavirenz binding increases the stabilities of the p51/p51 homodimer, the p66/p66 homodimer, and the p66/p51 heterodimer by 13.8, 9.2, and 7.5 kJ/mol, respectively. In contrast, binding of $TSAOe^3T$ decreases p66/p66 and p66/p51 stabilities by 13.4 and 16.7 kJ/mol, respectively (*9*); binding of BBNH and BBSH decreases the p66/p51 stability by 15.9 and 14.2 kJ/mol, respectively (*8*).

These disparate effects of NNRTI binding on dimerization can be reconciled by the thermodynamic linkage proposed in Scheme 1

Scheme 1: Thermodynamic Linkage of NNRTI Binding and Dimerization

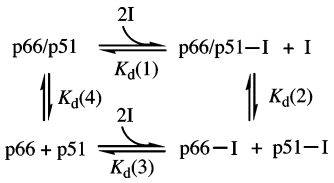

where I is NNRTI. Scheme 1 makes two assumptions: (1) the dimerization reaction is an equilibrium between dimer and folded monomer, and (2) NNRTI binds to dimer and folded monomer. The assumption of folded monomer is supported by the almost-identical far-UV circular dichroism spectra of three dimerization defective mutant p66 monomers and the wild-type p66/p51 heterodimer (*44*). In Scheme 1, $K_d(2)$ and $K_d(4)$ are the dissociation constants of the p66/p51 heterodimer measured in the presence and absence of efavirenz, respectively (Table 4)

$$K_d(2) = ([p66{-}I][p51{-}I])/([p66/p51{-}I][I]) \quad (13a)$$

$$K_d(4) = ([p66][p51])/[p66/p51] = K_d(p66/p51) \quad (13b)$$

and $K_d(1)$ and $K_d(3)$ are dissociation constants of the inhibitor from dimer and monomers, respectively.

$$K_d(1) = [p66/p51][I]/[p66/p51{-}I] \quad (13c)$$

$$K_d(3) = ([p66][I]/[p66{-}I])([p51][I]/[p51{-}I]) = K_d(p66{-}I)K_d(p51{-}I) \quad (13d)$$

The Gibbs free energy $\Delta G = 0$ around the closed path in Scheme 1. Substituting $\Delta G = -RT \ln K$ gives

$$-RT \ln K_d(2) - RT \ln K_d(3) = -RT \ln K_d(1) - RT \ln K_d(4) \quad (14)$$

so that

$$K_d(2)/K_d(4) = K_d(1)/K_d(3) \quad (15)$$

Analogous schemes and equations apply to p66/p66 and p51/p51 homodimers in the absence and presence of efavirenz. If NNRTI binding enhances dimerization, then $K_d(2)/K_d(4) < 1$ and $K_d(1) < K_d(3)$, indicating that the inhibitor binds tighter to the dimer than to the monomer. This is clearly the case for efavirenz, where $K_d(2)/K_d(4) = 0.0025$, 0.019, and 0.040 for the p51/p51 homodimer, the p66/p66 homodimer, and the p66/p51 heterodimer, respectively. Likewise, if NNRTI has no effect on dimerization, then eq 15 implies that the drug has equal affinity for the dimer and monomer. Finally, if NNRTI binding weakens dimerization, then $K_d(2)/K_d(4) > 1$ and $K_d(1) > K_d(3)$, indicating that the inhibitor binds tighter to the monomer than to the dimer. This is the case for $TSAOe^3T$, where $K_d(2)/K_d(4) = 180$ and 650 for the p66/p66 homodimer and p66/p51 heterodimer, respectively. Future sedimentation equilibrium studies are planned to measure K_d values of RT in the presence of NNRTIs with different effects on dimerization.

Effects of Efavirenz Binding on the Dimer Interface. The p66/p51 heterodimer has an asymmetric structure (*45*). The four subdomains of the p66 polymerase domain are arranged like a right hand: fingers, palm, thumb, and connection (Figure 6A). Despite identical sequences, the polymerase domains in the two subunits adopt different structures. The

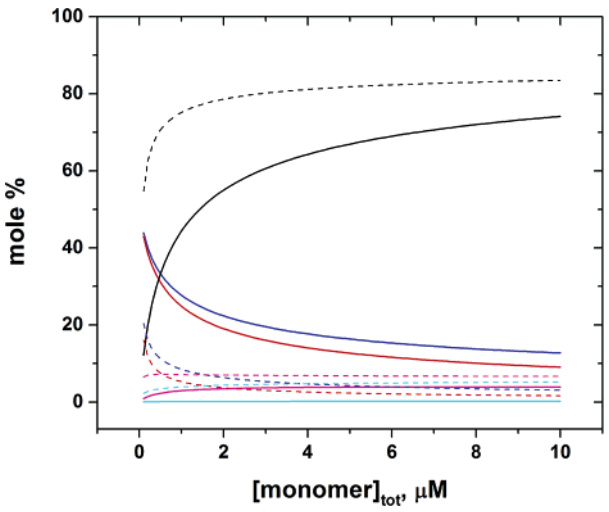

FIGURE 5: Relative amounts of monomeric and dimeric species (monomer concentration) in an equimolar mixture of p66 and p51 as a function of total monomer concentration in the (solid lines) absence and (dashed lines) presence of 25 μM efavirenz: black for p66/p51, red for p66, blue for p51, magenta for p66/p66, and cyan for p51/p51.

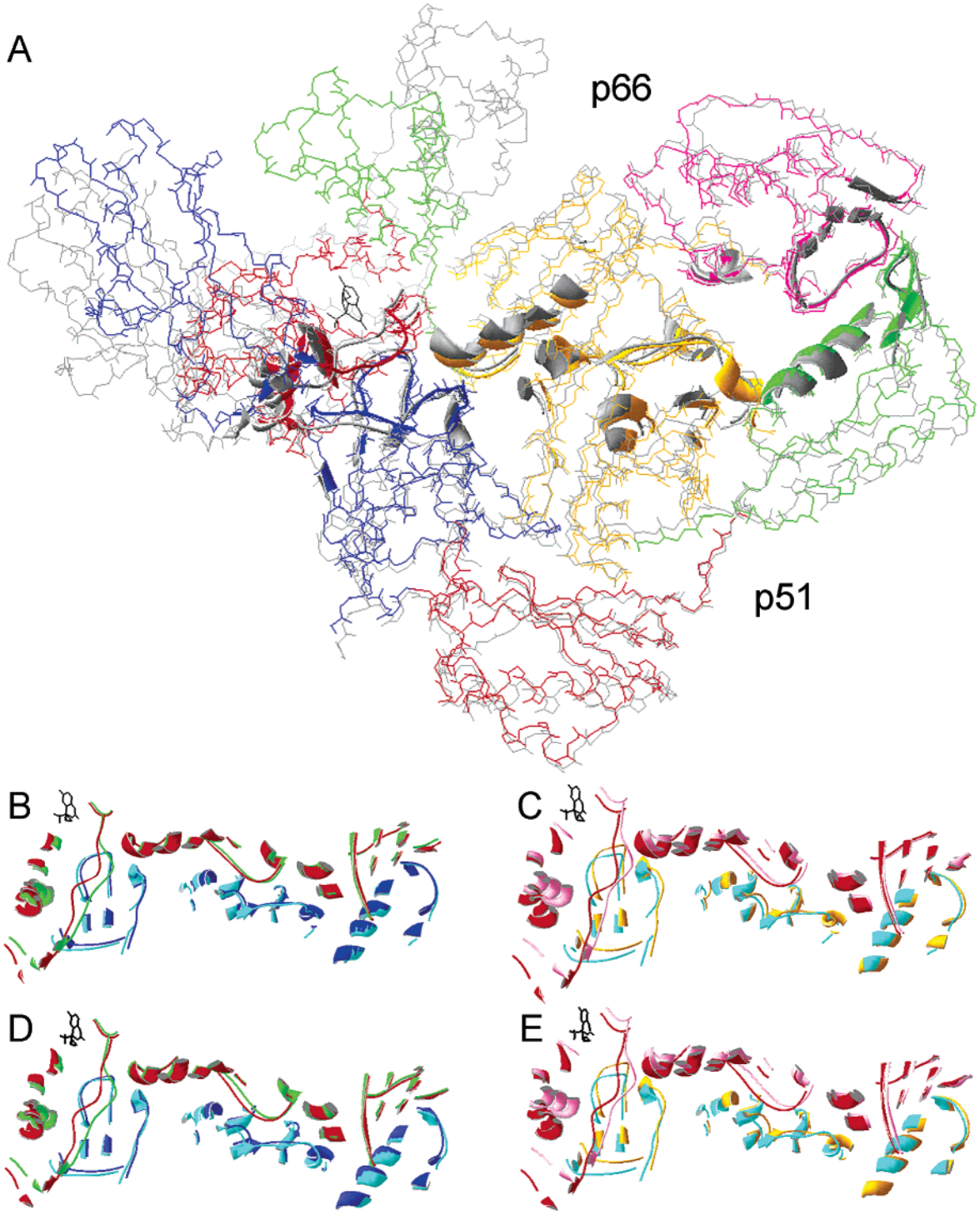

FIGURE 6: Ribbon diagrams of the subunit interface of HIV-1 p66/p51 RT in the absence and presence of efavirenz (black). (A) Front view of the superposition of RT (1DLO; polymerase subdomains of each subunit, blue for fingers, red for palm, green for thumb, and gold for connection; magenta for the p66 RNase H domain) and the RT−efavirenz complex (1IKW, gray). (B) Top view of interface residues from the superposition of RT (1DLO; green for p66 and blue for p51) and the RT−efavirenz complex (1IKW; red for p66 and cyan for p51). (C) Top view of interface residues from the superposition of RT (1HMV; pink for p66 and gold for p51) and the RT−efavirenz complex (1IKW; red for p66 and cyan for p51). (D) Top view of interface residues from the superposition of RT (1DLO; green for p66 and blue for p51) and the RT−efavirenz complex (1FK9; red for p66 and cyan for p51). (E) Top view of interface residues from the superposition of RT (1HMV; pink for p66 and gold for p51) and the RT−efavirenz complex (1FK9; red for p66 and cyan for p51).

folding of individual polymerase subdomains is similar in the two subunits, but the relative orientations of the subdomains as well as the subunit interfaces are different. The p66 polymerase domain has a large cleft between fingers and thumb subdomains, which forms the primer/template binding site (*46*). The polymerase active site and NNRTI binding pocket are in the palm subdomain (*17*). Several amino acid side chains that make contacts with efavirenz are also located in the dimer interface (*18*, *19*). The side chain of Y181 contacts the cyclopropyl-propynyl group of efavirenz, while the side chains of L100 and V179 contact the benzoxazin-2-one ring. In addition, the main chain

Table 5: Interface Parameters for HIV-1 RT Dimer Interfaces in the Absence and Presence of Efavirenz

	unliganded RT (1DLO)	unliganded RT (1HMV)	RT−efavirenz complex (1FK9)	RT−efavirenz complex (1IKW)
p66 interface ASA[a] (Å^2)	2499	2296	2312	2287
p51 interface ASA[a] (Å^2)	2605	2374	2428	2411
no. of H-bonds[b]	18	16	15	13
gap volume (Å^3)	15851	15017	14043	14201
no. of bridging waters	0	0	2	0

[a] ASA is the accessible surface area defined as the surface mapped out by the center of a 1.4 Å spherical probe rolled around the van der Waals surface of a protein. [b] Number of hydrogen bonds for residue determined by generating a set of possible positions for the H atom attached to a donor and searching for donor/acceptor pairs that fit the criteria.

carbonyl oxygen of K101 forms a hydrogen bond with the benzoxazin-2-one NH. The binding of efavirenz seems to induce several conformational changes in the structure of HIV-1 RT (*32*, *33*), including a change in the orientation of the p66 thumb subdomain (~40° rotation) that results in slight displacement of the p66 connection subdomain and RNase H domain and of the entire p51 subunit (*12*).

Figure 6 illustrates the conformational changes at the dimer interface of wild-type p66/p51 HIV-1 RT with all interface residues in a ribbon display. Because RT is quite flexible and crystallizes in different forms, dimer interfaces were examined in two structures each of the unliganded wild-type p66/p51 heterodimer, 1HMV (*32*) and 1DLO (*33*), and of the p66/p51−efaviernz complex, 1FK9 (*18*) and 1IKW (*19*). In panel A, the structure of the efavirenz complex 1IKW is superposed on the unliganded structure 1DLO. These two structures were chosen because of the similarity in crystallization conditions and spatial arrangement of the p66 fingers subdomain. The distortion of the p66 thumb subdomain as well as the shift in the orientation of the p66 fingers are clearly visible. Panel B presents another view of only the superposed dimer interfaces of these structures. Panel C presents the superposed dimer interfaces with the other wild-type p66/p51 structure 1HMV. In both panels B and C, the interface residues in the p66 palm subdomain and p51 fingers domain display discernible distortion in the efavirenz complex. The most dramatic structural changes are in the β5a−β5b sheets of the p66 subunit (D86−H96) and in the β7−β8 loop of the p51 subunit (I135−P140). The position of the interface residues in the p66 RNase H domain that contact the thumb subdomain of p51 is not much affected by the presence of efavirenz in either panel B or C. This is also true of the residues in the connection subdomains of both subunits that interact with one another. Finally, panels D and E present superposed dimer interfaces of the other efavirenz structure, 1FK9, with the two unliganded structures, 1DLO and 1HMV. Nearly identical distortions in the dimer interface are apparent in this efavirenz complex as well.

We explored the conformations of the dimer interface in the p66/p51 and p66/p51−efavirenz structures by further utilizing the Protein−Protein Interaction Server. The calculations revealed decreases in the number of hydrogen bonds and the gap volume in the efavirenz complexes (Table 5). Examination of the contributions of individual amino acid residues in the dimer interface indicates that the most striking differences between the p66/p51 heterodimer and the p66/p51−efavirenz complex occur in residues 90−92 (see Table S2 of the Supporting Information). First, V90 is no longer in the dimer interface of the complex according to the calculations. Second, G91 and L92 suffer an order of magnitude decrease in interface ASA in addition to loss of one or two hydrogen bonds, depending on the p66/p51 structure used for comparison. This observation is significant because none of these residues are located in the NNRTI binding pocket. Two residues that are in the binding pocket, K101 of the p66 subunit and G138 of the p51 subunit, also display noteworthy changes. Both residues gain a hydrogen bond in the p66/p51−efavirenz complex. All other differences in interface ASA between the structures seem to be relatively small. Thus, efavirenz binding clearly induces structural changes in the dimer interface of the p66/p51 heterodimer, which may account at least in part for the increased subunit affinity.

SUPPORTING INFORMATION AVAILABLE

Fringe factor calculation and a table of dimer interface residues (Table S2). This material is available free of charge via the Internet at http://pubs.acs.org.

REFERENCES

1. Restle, T., Müller, B., and Goody, R. S. (1990) Dimerization of human immunodeficiency virus type 1 reverse transcriptase, *J. Biol. Chem. 265*, 8986−8988.
2. Restle, T., Müller, B., and Goody, R. S. (1992) RNase H activity of HIV reverse transcriptase is confined exclusively to the dimeric forms, *FEBS Lett. 300*, 97−100.
3. Le Grice, S. F. J., Naas, T., Wohlgensinger, B., and Schatz, O. (1991) Subunit-selective mutagenesis indicates minimal polymerase activity in heterodimer-associated p51 HIV-1 reverse transcriptase, *EMBO J. 10*, 3905−3911.
4. Bavand, M. R., Wagner, R., and Richmond, T. J. (1993) HIV-1 reverse transcriptase: Polymerization properties of the p51 homodimer compared to the p66/p51 heterodimer, *Biochemistry 32*, 10543−10552.
5. Becerra, S. P., Kumar, A., Lewis, M. S., Widen, S. G., Abbotts, J., Karawya, E. M., Hughes, S. H., Shiloach, J., and Wilson, S. H. (1991) Protein−protein interactions of HIV-1 reverse transcriptase: Implication of central and C-terminal regions in subunit binding, *Biochemistry 30*, 11707−11719.
6. Divita, G., Rittinger, K., Restle, T., Immendörfer, U., and Goody, R. S. (1995) Conformational stability of dimeric HIV-1 and HIV-2 reverse transcriptases, *Biochemistry 34*, 16337−16346.
7. Lebowitz, J., Kar, S., Braswell, E., McPherson, S., and Richard, D. L. (1994) Human immunodeficiency virus-1 reverse transcriptase heterodimer stability, *Protein Sci. 3*, 1374−1382.
8. Sluis-Cremer, N., Arion, D., and Parniak, M. A. (2002) Destabilization of the HIV-1 reverse transcriptase dimer upon interaction with *N*-acyl hydrazone inhibitors, *Mol. Pharmacol. 62*, 398−405.
9. Sluis-Cremer, N., Dmitrienko, G. I., Balzarini, J., Camarasa, M.-J., and Parniak, M. A. (2000) Human immunodeficiency virus type I reverse transcriptase dimer destablilization by 1-{spiro[4′-amino-2′,2′-dioxo-1′,2′-oxathiole-5′,3′-[2′,5′-bis-*O*-(*tert*-butyldimethylsilyl)-β-D-ribofuranosyl]]}-3-ethylthymine, *Biochemistry 39*, 1427−1433.
10. Cabodevilla, J. F., Odriozola, L., Santiago, E., and Martinez-Irujo, J. J. (2001) Factors affecting the dimerization of the p66 form of HIV-1 reverse transcriptase, *Eur. J. Biochem. 268*, 1163−1172.
11. Mao, C., Sudbeck, E. A., Venkatachalam, T. K., and Ucken, F. M. (2000) Structure-based drug design of non-nucleoside inhibitors

for wild-type and drug-resistant HIV reverse transcriptase, *Biochem. Pharmacol. 60*, 1251−1265.
12. Sluis-Cremer, N., Temiz, N. A., and Bahar, I. (2004) Conformational Changes in HIV-1 Reverse Transcriptase Induced by Nonnucleoside Reverse Transcriptase Inhibitor Binding, *Curr. HIV Res. 2*, 323−332.
13. Borkow, G., Fletcher, R. S., Barnard, J., Arion, D., Motakis, D., Dmitrienko, G. I., and Parniak, M. A. (1997) Inhibition of the ribonuclease H and DNA polymerase activities of HIV-1 reverse transcriptase by *N*-(4-*tert*-butylbenzoyl)-2-hydroxy-α-naphthaldehyde hydrazone, *Biochemistry 36*, 3179−3185.
14. Tachedjian, G., Orlova, M., Sarafianos, S. G., Arnold, E., and Goff, S. P. (2001) Nonnucleoside reverse transcriptase inhibitors are chemical enhancers of dimerization of the HIV type 1 reverse transcriptase, *Proc. Natl. Acad. Sci. U.S.A. 98*, 7188−7193.
15. Merluzzi, V. J., Hargrave, K. D., Labadia, M., Grozinger, K., Skoog, M., Wu, J. C., Shih, C.-K., Eckner, K., Hattox, S., Adams, J., Rosenthal, A. S., Faanes, R., Eckner, R. J., Koup, R. A., and Sutton, J. L. (1990) Inhibition of HIV-1 replication by a nonnucleoside reverse transcriptase inhibitor, *Science 250*, 1411−1413.
16. Spence, R. A., Kati, W. M., Anderson, K. S., and Johnson, K. A. (1995) Mechanism of inhibition of HIV-1 reverse transcriptase by nonnucleoside inhibitors, *Science 267*, 988−993.
17. Kohlstaedt, L. A., Wang, J., Friedman, J. M., Rice, P. A., and Steitz, T. A. (1992) Crystal structure at 3.5 Å resolution of HIV-1 reverse transcriptase complexed with an inhibitor, *Science 256*, 1783−1790.
18. Ren, J., Milton, J., Weaver, K. L., Short, S. A., Stuart, D. I., and Stammers, D. K. (2000) Structural basis for the resilience of efavirenz (DMP-266) to drug resistance mutations in HIV-1 reverse transcriptase, *Structure 8*, 1089−1094.
19. Lindberg, J., Sigurdsson, S., Löwgren, S., Andersson, H. O., Sahlberg, C., Noréen, R., Fridborg, K., Zhang, H., and Unge, T. (2002) Structural basis for the inhibitory efficacy of efavirenz (DMP-266), MSC194 and PNU142721 towards the HIV-1 RT K103N mutant, *Eur. J. Biochem. 269*, 1670−1677.
20. Tachedjian, G., Moore, K. L., Goff, S. P., and Sluis-Cremer, N. (2005) Efavirenz enhances the proteolytic processing of an HIV-1 pol polyprotein precursor and reverse transcriptase homodimer formation, *FEBS Lett. 579*, 379−384.
21. Le Grice, S. F. J., Cameron, C. E., and Benkovic, S. J. (1995) Purification and characterization of human immunodeficiency virus type 1 reverse transcriptase, *Methods Enzymol. 262*, 130−144.
22. van Holde, K. E., and Baldwin, R. L. (1958) Rapid attainment of sedimentation equilibrium, *J. Phys. Chem. 62*, 734−743.
23. XLGraph. http://www.jphilo.mailway.com/download.htm.
24. Gill, S. C., and von Hippel, P. H. (1989) Calculation of protein extinction coefficients from amino acid sequence data, *Anal. Biochem. 182*, 319−326.
25. Ignatov, M. E., Berdis, A. J., Le Grice, S. F. J., and Barkley, M. D. (2005) Attenuation of DNA replication by HIV-1 reverse transcriptase near the central termination sequence, *Biochemistry 44*, 5346−5356.
26. PROTCALC, MIXEDFIT, HETERFIT, AND MWCALC. http://rasmb.bbri.org/rasmb/windows/programs-Les_Holladay/.
27. Makhatadze, G. I., Medvedkin, V. N., and Privalov, P. L. (1990) Partial molar volume of polypeptides and their constituent groups in aqueous solution over a broad temperature range, *Biopolymers 30*, 1001−1010.
28. Gekko, K., and Timasheff, S. N. (1981) Mechanism of protein stabilization by glycerol: Preferential hydration in glycerol-water mixtures, *Biochemistry 20*, 4667−4676.
29. Osbourne, J. C., Jr., Schaefer, E. J., Powell, G. M., Lee, N. S., and Zech, L. A. (1984) Molecular properties of radioiodinated apolipoprotein A-I, *J. Biol. Chem. 259*, 347−353.
30. Lewis, M. S., and Reily, M. M. (2004) Estimation of weights for various methods of the fitting of equilibrium data from the analytical ultracentrifuge, *Methods Enzymol. 384*, 232−242.
31. Press, W. H., Flannery, B. P., Teukolsky, S. A., and Vetterling, W. T. (1989) *Numerical Recipes in Pascal*, Cambridge University Press, New York.
32. Rodgers, D. W., Gamblin, S. J., Harris, B. A., Ray, S., Culp, J. S., Hellmig, B., Woolf, D. J., Debouck, C., and Harrison, S. C. (1995) The structure of unliganded reverse transcriptase from the human immunodeficiency virus type 1, *Proc. Natl. Acad. Sci. U.S.A. 92*, 1222−1226.
33. Hsiou, Y., Ding, J., Das, K., Clark, A. D., Jr., Hughes, S. H., and Arnold, E. (1996) Structure of unliganded HIV-1 reverse transcriptase at 2.7 Å resolution: Implications of conformational changes for polymerization and inhibition mechanisms, *Structure 4*, 853−857.
34. Deep View/Swiss-Pdb Viewer. http://www.expasy.org/spdbv.
35. Protein−Protein Interaction Server. http://www.biochem.ucl.ac.uk/bsm/PP/server.
36. Holladay, L. A., and Sophianopoulos, A. J. (1972) Nonideal associating systems, *J. Biol. Chem. 247*, 427−439.
37. Peletskaya, E. N., Boyer, P. L., Kogon, A. A., Clark, P., Kroth, H., Sayer, J. M., Jerina, D. M., and Hughes, S. H. (2001) Cross-linking of the fingers subdomain of human immunodeficiency virus type 1 reverse transcriptase to template-primer, *J. Virol. 75*, 9435−9445.
38. Peletskaya, E. N., Kogon, A. A., Tuske, S., Arnold, E., and Hughes, S. H. (2004) Nonnucleoside inhibitor binding affects the interactions of the fingers subdomain of human immunodeficiency virus type 1 reverse transcriptase with DNA, *J. Virol. 78*, 3387−3397.
39. Rausch, J. W., Sathyanarayana, B. K., Bona, M. K., and Le Grice, S. F. J. (2000) Probing contacts between the ribonuclease H domain of HIV-1 reverse transcriptase and nucleic acid by site-specific photocross-linking, *J. Biol. Chem. 275*, 16015−16022.
40. Kensch, O., Restle, T., Wöhrl, B. M., Goody, R. S., and Steinhoff, H.-J. (2000) Temperature-dependent equilibrium betweeen the open and closed conformation of the p66 subunit of HIV-1 reverse transcriptase revealed by site-directed spin labeling, *J. Mol. Biol. 301*, 1029−1039.
41. Rothwell, P. J., Berger, S., Kensch, O., Felekyan, S., Antonik, M., Wöhrl, B. M., Restle, T., Goody, R. S., and Seidel, C. A. M. (2003) Multiparameter single-molecule fluorescence spectroscopy reveals heterogeneity of HIV-1 reverse transcriptase:primer/template complexes, *Proc. Natl. Acad. Sci. U.S.A. 100*, 1655−1660.
42. Young, S. D., Britcher, S. F., Tran, L. O., Payne, L. S., Lumma, W. C., Lyle, T. A., Huff, J. R., Anderson, P. S., Olsen, D. B., Carroll, S. S., Pettibone, D. J., O'Brien, J. A., Ball, R. G., Balani, S. K., Lin, J. H., Chen, I.-W., Schleif, S. A., Sardana, V. V., Long, W. J., Byrnes, V. W., and Emini, E. A. (1995) L-743,726 (DMP-266): A novel, highly potent nonnucleoside inhibitor of the human immunodeficiency virus type 1 reverse transcriptase, *Antimicrob. Agents Chemother. 39*, 2602−2605.
43. Maga, G., Ubiali, D., Salvetti, R., Pregnolato, M., and Spadari, S. (2000) Selective interaction of the human immunodeficiency virus type 1 reverse transcriptase nonnucleoside inhibitor efavirenz and its thio-substituted analog with different enzyme−substrate complexes, *Antimicrob. Agents Chemother. 44*, 1186−1194.
44. Tachedjian, G., Radzio, J., and Sluis-Cremer, N. (2005) Relationship between enzymatic activity and dimeric structure of recombinant HIV-1 reverse transcriptase, *Proteins: Struct., Funct., Bioinf. 60*, 5−13.
45. Wang, J., Smerdon, S. J., Jäger, J., Kohlstaedt, L. A., Rice, P. A., Friedman, J. M., and Steitz, T. A. (1994) Structural basis of asymmetry in the human immunodeficiency virus type 1 reverse transcriptase heterodimer, *Proc. Natl. Acad. Sci. U.S.A. 91*, 7242−7246.
46. Jacobo-Molina, A., Ding, J., Nanni, R. G., Clark, A. D., Jr., Lu, X., Tantillo, C., Williams, R. L., Kamer, G., Ferris, A. L., Clark, P., Hizi, A., Hughes, S. H., and Arnold, E. (1993) Crystal structure of human immunodeficiency virus type 1 reverse transcriptase complexed with double-stranded DNA at 3.0 Å resolution shows bent DNA, *Proc. Natl. Acad. Sci. U.S.A. 90*, 6320−6324.

BI051915Z